Published in final edited form as:
ACS Appl Mater Interfaces. 2016 November 23; 8(46): 31935–31940. doi:10.1021/acsami.6b10611.

Shape Memory Cellulose-based Photonic Reflectors

André Espinha[†,1], **Giulia Guidetti**[‡], **María C. Serrano**[§], **Bruno Frka-Petesic**[‡], **Ahu Gumrah Parry**[‡], **Wadood Y. Hamad**[‖], **Álvaro Blanco**[†], **Cefe López**[*,†], and **Silvia Vignolini**[*,‡]

[†]Instituto de Ciencia de Materiales de Madrid, Consejo Superior de Investigaciones Científicas, Calle Sor Juana Inés de la Cruz, 3, Cantoblanco, 28049 Madrid, Spain

[‡]Department of Chemistry, University of Cambridge, Lensfield Road, Cambridge CB2 1EW UK

[§]Hospital Nacional de Parapléjicos, Servicio de Salud de Castilla La Mancha, Finca La Peraleda s/n, 45071 Toledo, Spain

[‖]FP Innovation, Departments of Chemistry and Chemical & Biological Engineering, University of British Columbia, 2665 East Mall, Vancouver, BC V6T 1Z4 Canada

Abstract

Bio-polymer based composites enable to combine different functionalities using renewable materials and cost-effective routes. Here we fabricate novel thermoresponsive photonic films combining cellulose nanocrystals (CNCs) with a polydiolcitrate elastomer exhibiting shape memory properties. In this composite, CNCs provide an intense structural coloration and improve the overall mechanical cohesion, while the elastomer drastically reduces the intrinsic brittleness of the photonic cellulose film and enables the shape memory effect. The fabricated samples are characterized by polarized optical microscopy, scanning electron microscopy and thermomechanical programming. The obtained results demonstrate that this hybrid material retains its chiral nematic structure and performs shape recovery in thermomechanical experiments thus widening the functionality of the independent components.

Keywords

cellulose nanocrystals; cholesteric; polydiolcitrates; shape memory; biomimetic

Plastics are key materials in many aspects of daily life, ranging from packaging, to construction, to medical applications. The replacement of conventional plastics with biocompatible and biodegradable ones enables to exploit the versatility of polymeric materials with the advantage of using sustainable fabrication approaches. Within this context, photonic materials produced by self-assembly of biopolymers are receiving growing interest in the materials community.1–3 Many photonic structures with diverse optical responses have been produced using a large variety of biomaterials and fabrication methods.

[*]**Corresponding Authors**: C.L.: c.lopez@csic.es; S.V.: sv319@cam.ac.uk.
[1]Institut de Ciència de Materials de Barcelona, Consejo Superior de Investigaciones Científicas, Carrer dels Til·lers S/N, Campus de la UAB, 08193 Bellaterra, Barcelona, Spain.

Author Contributions
The manuscript was written through contributions of all authors. All authors have given approval to the final version of the manuscript.

Europe PMC Funders Author Manuscripts

4–6 However, there are limitations on the different functionalities that can be achieved using only sustainable and biocompatible polymers. As an example, cellulose-based photonic structures can provide strong, intense colorations but they are generally very brittle.7 The addition of organic and inorganic matrices to such cellulose structures improves their mechanical properties but either comports the loss of the photonic effect or reduces the fully biocompatibility of the final composite.8

Here we present a hybrid cellulose-based photonic structure exhibiting shape memory, fabricated by combining cellulose nanocrystals (CNCs) photonic films with a polydiolcitrate elastomer.9 In particular, we directly impregnate and embed colored CNC films with hydroxyl-dominant poly(dodecanediol-co-citrate) (PDDC-HD).10 The CNCs contribute both to the structural coloration of the film and to its overall mechanical cohesion, while the PDDC-HD provides both flexibility and reduced brittleness due to its elastomeric properties and adds functionality by introducing the shape memory effect.

Shape memory polymers11 have been implemented in the design of a large variety of thermomechanically programmable components with interest in photonics.12–15 On their turn, polydiolcitrate elastomers have drawn attention due to the possibility of programming structural features at the nanoscale16 or achieving shape programmable gain media.17 However, shape memory polymers, when combined with different types of cellulose sources, have produced only amorphous, colorless composites with enhanced mechanical response. To cite some examples, Chiu and co-workers reported microfibrillated cellulose-poly(propylene carbonate) composites with shape memory and self-healing properties.18 Sonseca et al. investigated the feasibility of customizing the stiffness and toughness of poly(mannitol sebacate) by introducing CNCs.19 Similarly, composites in which CNCs improved the fixity ratio in poly(ester-urethane) and polycaprolactone and polyethylene glycol have been described (20) and (21), respectively.

Our approach consists in the fabrication of thermoresponsive optically active composites, as summarized in the following steps: (i) CNC photonic film fabrication, (ii) impregnation in the PDDC-HD prepolymer, and (iii) partial thermal treatment for crosslinking the prepolymer, thus providing the sample with shape memory effect. Its programmable features are then assessed through thermomechanical cycling. A schematic diagram of the fabrication procedure can be found in the Supporting Information - SI (Figure S1).

In the first step the free standing CNC photonic films are fabricated via evaporation induced self-assembly (EISA),22 following the protocol presented in the Experimental Section (SI). Three CNC suspensions with different heat treatment are used to fabricate CNC films with colorations going from red, to green and blue, by controlling the desulfation and ionic strength adjustment.23, 24 The PDDC-HD prepolymer is synthesized by mixing citric acid and 1,12-dodecanediol, and subsequently diluted in ethanol to favor its diffusion into the swelling CNC film. In order to further facilitate such diffusion, the CNC films are immersed in the prepolymer overnight. After about 15 hours soaking, the films are removed, drained from the prepolymer and left to dry in ambient conditions to allow complete ethanol evaporation. At this stage the hybrid films have a slightly opaque appearance induced by light scattering from non-crosslinked prepolymer microdomains.13

For all the fabrication stages, the obtained films are characterized by polarized optical microscopy,25 as described in the experimental section (SI). Optical micrographs and reflectivity spectra of chiral nematic cellulose films before and after the prepolymer impregnation (i.e. before curing) are shown for initially blue, green and red CNC films in Figure 1a and 1b, respectively. As expected for CNC chiral nematic films, left circularly polarized light is reflected in a specific spectral region, due to the stacking periodicity induced by their chiral nematic structure.26

The prepolymer impregnation does not affect the chiral nematic ordering of the CNCs and leads to a consistent redshift, for all the investigated spectral regions (Figure 1). Such a red-shift clearly demonstrates the penetration of the prepolymer into the swollen CNC films, either by affecting the average optical index of the infiltrated CNCs film ($n_{PDDC\text{-}HD}$ = 1.522) or by the macroscopic swelling of the films. The latter effect is also supported by a broadening of the reflection peaks as well as by SEM analysis of the films after curing (see below).

Representative spectra of the three samples are collected before and after the infiltration and shown in Figure 1b. As previously mentioned, the reflection peak is observed only using a circularly-left polarizing filter, assuring that the axes of the chiral nematic structure are perpendicular to the film surface.26 In order to take into account the intrinsic multi-domain nature of the CNC films, we measure several spectra in different positions; Table 1 reports the average spectral position of the reflectance maximum (in the left circularly polarized channel) (λ_{av}) before and after the impregnation. After the impregnation process, λ_{av} undergoes a displacement of approximately 20% towards red-shifted wavelengths for all the samples. Interestingly, the standard deviation of the measured λ_{av} increased after the infiltration and can result from an inhomogeneous infiltration throughout the CNC film thickness. Moreover, the swelling of the CNC films by the prepolymer seems to be reduced in the samples that were more exposed to heat treatment, which are also those expected to have stronger van der Waals attractive interactions.24, 27

In a second stage, the impregnated films are subjected to a partial thermal treatment in order to crosslink the PDDC-HD polymeric chains and provide the shape memory functionality to the final samples. The samples were kept flat during this step in order to fix it as the permanent shape of the films. The optical characterization of a representative cured film is reported in Figure 2. The films maintain the color appearance (Figure 2a) and a strong reflection peak is observed in the left circularly polarized channel (LCP) (Figure 2b), which confirms that the final hybrid material retains its chiral nematic structure. However, the presence of an increased signal in the right polarization channel (RCP), mostly on localized defects of the cholesteric structure, indicates that the infiltration process slightly affects the orientation of the axes of the chiral nematic domains. A comparison of the average positions of the reflection peak at the different steps of the fabrication process is reported in Figure 2c, showing no noticeable color shift after curing.

In order to characterize the morphology of the CNC/PDDC-HD hybrid materials after curing, the cross-section of the films was investigated using scanning electron microscopy (SEM), as reported on Figure 3 and Figure S2 (SI). From the SEM we observe that the

PDDC-HD forms a thick layer on both side of the CNC film (cf. Figure S2 of SI), increasing the total thickness of the CNC film from ~4.5μm to ~35μm (CNC film sandwiched between PDDC-HD layers), while the CNC layer itself seems on average thicker (~6.5μm), indicating that the PDDC-HD is infiltrated in the CNC layer. High magnification SEM imaging of the cross-section enables to recognize the Bouligand arches further confirming the retain of cholesteric structures in the cellulose film.28 A systematic and statistical analysis of the cholesteric pitch, measured as twice the pattern periodicity, shows a pitch increase of ~16% after the PDDC-HD impregnation, as reported in Table 2.

Finally, Table 2 shows the estimation of the product $n_{av} * t_{av}$ (product of the average optical index and the CNC cholesteric thickness) using the Fabry-Perot oscillations observed in the reflection spectra. The observed increase of $n_{av} * t_{av}$ confirms the information regarding the PDDC-HD incorporation in the CNC film. However, these oscillations interfere in the presence of the additional PDDC-HD layers and become difficult to detect on samples after impregnation and curing.

In order to assess the shape memory properties of the CNC/PDDC-HD hybrid materials, thermomechanical programming was carried out on the cured samples. Samples stored at room temperature were used as follows: first, they were heated above their melting transition temperature (T_{trans} ~ 30 °C) using a heat gun, then rolled up while maintained above T_{trans}, and finally left to cool down at room temperature, holding it mechanically in that shape to allow the material to solidify in a rolled configuration (i.e. approximately 10 min till complete solidification of the polymer). This enables us to provide a new rigid shape to the material (temporary shape), and test the recovery of the permanent shape (memorized during the initial curing) by applying a mild heat stress. Such tests are reported in Figure 4 (and by the corresponding videos in SI), where the fabricated CNC/PDDC-HD thin films exhibited shape recovery. Moreover, the films were able to restore their permanent shape regardless of the gravity bias. The optical characteristics of the films were maintained during the thermal cycle, while only a transparency increase at high temperature was observed above T_{trans}.13

Finally, the overall mechanical performances of the hybrid CNC/PDDC-HD composite can be tuned on demand. As the effective Young modulus depends on the relative thickness of the middle (CNC-rich) and outer (PDDC-HD based) layers. Using a simplified model of high Young modulus CNC film (usually around 2-6 GPa)29 surrounded by lower Young modulus PDDC-HD elastomer (2-20 MPa),13 we estimated for the example of the hybrid material in Figure S2 an effective Young modulus around ~40 MPa (calculated in a bending geometry, details in SI), much lower than for a brittle, pure CNC film and about 2.7 times larger than pure PDDC-HD.

Most importantly, the high cohesion of the hybrid CNC/PDDC-HD material is assured by the infiltration of the PDDC-HD inside the CNC layer and, in this way, a functional and responsive material, bridging structural coloration and shape memory properties, is achieved. Indeed, other investigated routes, such as direct co-assembly of the CNCs in the shape memory prepolymer and direct casting of the CNCs onto a shape memory polymer substrate either led to no structural coloration, or delamination.

In summary, we presented a proof of concept for the fabrication of thermoresponsive chiral nematic photonic materials. The fabricated hybrid materials are based on cellulose nanocrystal films impregnated with and embedded in a shape memory polymer of hydroxyl-dominant poly(dodecanediol-co-citrate). We studied the evolution of the optical properties for each of the fabrication steps, demonstrating the retaining of the chiral nematic structure typical of the CNC films in the PDDC-HD matrix. Besides the optical and thermomechanical properties, useful for detection or actuation, this functional composite performs at clinically relevant temperatures (room to body temperature), due to the working temperature at which the shape memory effect in PDDC-HD is triggered.

Supplementary Material

Refer to Web version on PubMed Central for supplementary material.

Acknowledgment

This work was partially funded by EU FP7 NoE Nanophotonics4Energy grant No. 248855, the Spanish MINECO project MAT2015-68075 (SIFE2), Comunidad de Madrid S2013/MIT-2740 (PHAMA_2.0) program. All the authors acknowledge the Royal Society (2014/R2-IE140719). AE was supported by the FPI PhD program from the MICINN. SV, BFP and AGP are funded by the BBSRC David Phillips fellowship [BB/K014617/1], and the ERC-2014-STG H2020 639088. MCS acknowledges the Instituto de Salud Carlos III of Spain for a Miguel Servet I contract (MS13/00060).

References

(1). Hamley IW. Liquid crystal phase formation by biopolymers. Soft Matter. 2010; 6:1863–1871.

(2). Wegst U, Bai H, Saiz E, Tomsia A, Ritchie R. Bioinspired structural materials. Nat Mat. 2015; 14:23–36.

(3). Dumanli A, Van der Kooij H, Kamita G, Reisner E, Baumberg J, Steiner U, Vignolini S. Digital color in cellulose nanocrystal films. ACS Appl Mater Interfaces. 2014; 6:12302–12306. [PubMed: 25007291]

(4). Giese M, Blusch L, Khan M, Hamad W, MacLachlan M. Responsive Mesoporous Photonic Cellulose Films by Supramolecular Cotemplating. Angew Chem Int Edit. 2014; 53:8880–8884.

(5). Khan M, Hamad W, MacLachlan M. Tunable mesoporous bilayer photonic resins with chiral nematic structures and actuator properties. Adv Mat. 2014; 26:2323–2328.

(6). Shopsowitz K, Stahl A, Hamad W, MacLachlan M. Hard Templating of Nanocrystalline Titanium Dioxide with Chiral Nematic Ordering. Angew Chem Int Edit. 2012; 51:6886–6890.

(7). Canché-Escamilla G, Rodriguez-Laviada J, Cauich-Cupul J, Mendizábal E, Puig J, Herrera-Franco P. Flexural, impact and compressive properties of a rigid-thermoplastic matrix/cellulose fiber reinforced composites. Compos Part A-Appl S. 2002; 33:539–549.

(8). Kelly J, Shopsowitz K, Ahn J, Hamad W, MacLachlan M. Chiral nematic stained glass: controlling the optical properties of nanocrystalline cellulose-templated materials. Langmuir. 2012; 28:17256–17262. [PubMed: 23186125]

(9). Yang J, Webb A, Ameer G. Novel citric acid-based biodegradable elastomers for tissue engineering. Adv Mat. 2004; 16:511–516.

(10). Serrano M, Carbajal L, Ameer G. Novel biodegradable shape-memory elastomers with drug-releasing capabilities. Adv Mat. 2011; 23:2211–2215.

(11). Behl M, Razzaq M, Lendlein A. Multifunctional Shape-Memory Polymers. Adv Mat. 2010; 22:3388–3410.

(12). Tippets C, Li Q, Fu Y, Donev E, Zhou J, Turner S, Jackson A, Ashby V, Sheiko S, Lopez R. Dynamic Optical Gratings Accessed by Reversible Shape Memory. ACS Appl Mater Interfaces. 2015; 7:14288–14293. [PubMed: 26081101]

(13). Schneider N, Zeiger C, Kolew A, Schneider M, Leuthold J, Hölscher H, Worgull M. Nanothermoforming of hierarchical optical components utilizing shape memory polymers as active molds. Opt Mater Express. 2014; 4:1895–1902.

(14). Fang Y, Leo S, Ni Y, Yu L, Qi P, Wang B, Basile V, Taylor C, Jiang P. Optically Bistable Macroporous Photonic Crystals Enabled by Thermoresponsive Shape Memory Polymers. Adv Opt Mater. 2015; 3:1509–1516.

(15). Fang Y, Ni Y, Leo S, Taylor C, Basile V, Jiang P. Reconfigurable photonic crystals enabled by pressure-responsive shape-memory polymers. Nat Commun. 2015; 6

(16). Espinha A, Serrano M, Blanco A, López C. Thermoresponsive Shape-Memory Photonic Nanostructures. Adv Opt Mat. 2014; 2:516–521.

(17). Espinha A, Serrano M, Blanco A, López C. Random Lasing in Novel Dye-Doped White Paints with Shape Memory. Adv Opt Mat. 2015; 3:1080–1087.

(18). Qi X, Yang G, Jing M, Fu Q, Chiu F. Microfibrillated cellulose-reinforced bio-based poly(propylene carbonate) with dual shape memory and self-healing properties. J Mater Chem A. 2014; 2:20393–20401.

(19). Sonseca A, Camarero-Espinosa S, Peponi L, Weder C, Foster E, Kenny J, Giménez E. Mechanical and shape-memory properties of poly(mannitol sebacate)/cellulose nanocrystal nanocomposites. J Polym Sci Pol Chem. 2014; 52:3123–3133.

(20). Navarro-Baena I, Kenny J, Peponi L. Thermally-activated shape memory behaviour of bionanocomposites reinforced with cellulose nanocrystals. Cellulose. 2014; 21:4231–4246.

(21). Liu Y, Li Y, Yang G, Zheng X, Zhou S. Multi-stimulus-responsive shape-memory polymer nanocomposite network cross-linked by cellulose nanocrystals. ACS Appl Mater Interfaces. 2015; 7:4118–4126. [PubMed: 25647407]

(22). Lagerwall J, Schütz C, Salajkova M, Noh J, Park J, Scalia G, Bergström L. Cellulose nanocrystal-based materials: from liquid crystal self-assembly and glass formation to multifunctional thin films. NPG Asia Mater. 2014; 6:e80.

(23). Beck S, Bouchard J, Berry R. Controlling the Reflection Wavelength of Iridescent Solid Films of Nanocrystalline Cellulose. Biomacromolecules. 2011; 12:167–172. [PubMed: 21133373]

(24). Parker R, Frka-Petesic B, Guidetti G, Kamita G, Consani G, Abell C, Vignolini S. Hierarchical Self-assembly of Cellulose Nanocrystals in a Confined Geometry. ACS Nano. 2016

(25). Vignolini S, Thomas M, Kolle M, Wenzel T, Rowland A, Rudall P, Baumberg J, Glover B, Steiner U. Directional scattering from the glossy flower of Ranunculus: how the buttercup lights up your chin. J R Soc Interface. 2012; 9:1295–1301. [PubMed: 22171065]

(26). de Vries H. Rotatory power and other optical properties of certain liquid crystals. Acta Cryst. 1951; 4:219–226.

(27). Beck S, Bouchard J, Chauve G, Berry R. Controlled production of patterns in iridescent solid films of cellulose nanocrystals. Cellulose. 2013; 20:1401–1411.

(28). Neville A, Gubb D, Crawford R. A new model for cellulose architecture in some plant cell walls. Protoplasma. 1976; 90:307–317.

(29). Bardet R, Belgacem N, Bras J. Flexibility and color monitoring of cellulose nanocrystal iridescent solid films using anionic or neutral polymers. ACS Appl Mater Interfaces. 2015; 7:4010–4018. [PubMed: 25552332]

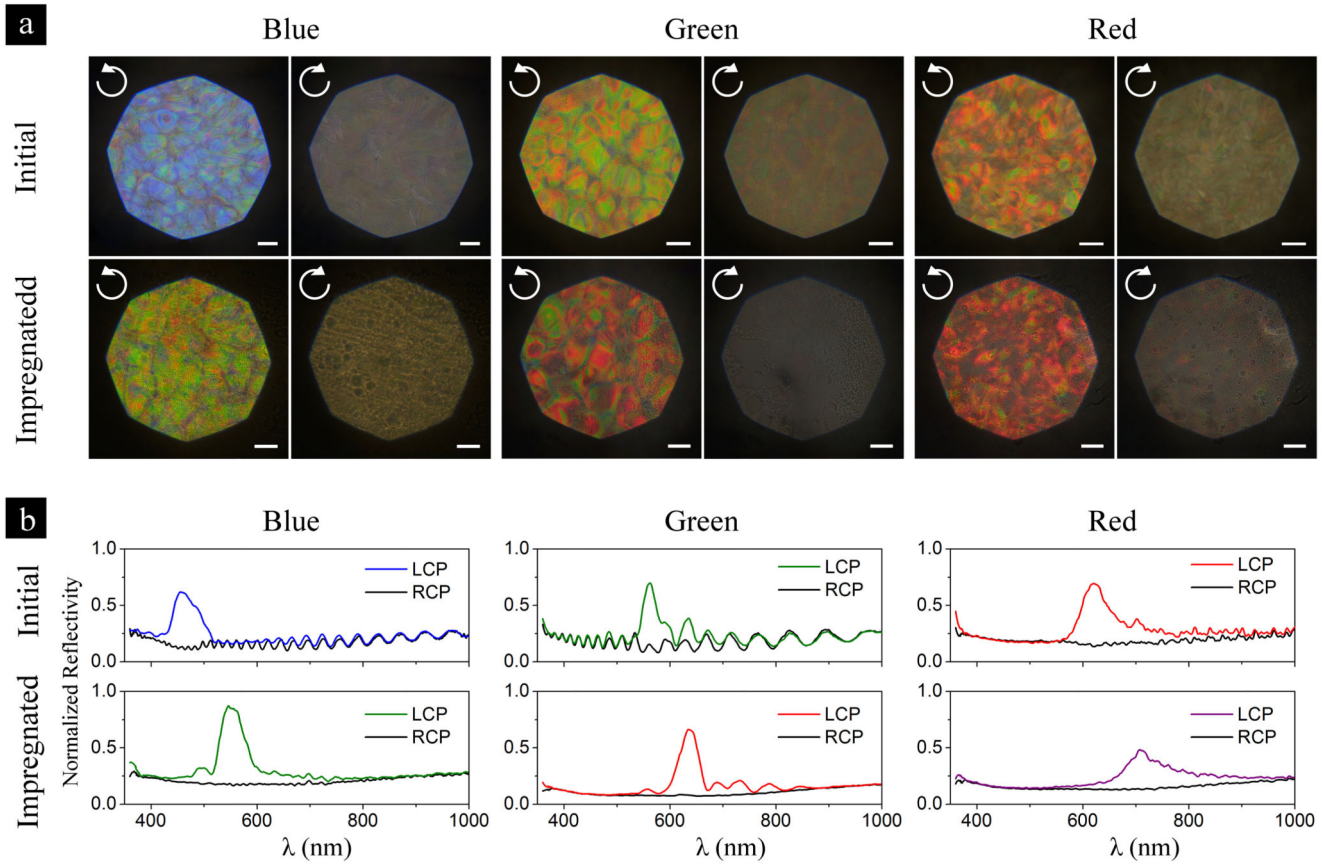

Figure 1.

(a) Polarized optical microscopy images, for left and right circular polarization, for three CNC films initially reflecting in the blue, green and red (top line) and then redshifted to the green, red and infra-red after prepolymer infiltration (bottom line). Scale bar corresponds to 50 μm. (b) Corresponding reflection spectra, for both polarizations, before (top line) and after (bottom line) the infiltration with prepolymer, prior to curing.

Europe PMC Funders Author Manuscripts

Europe PMC Funders Author Manuscripts

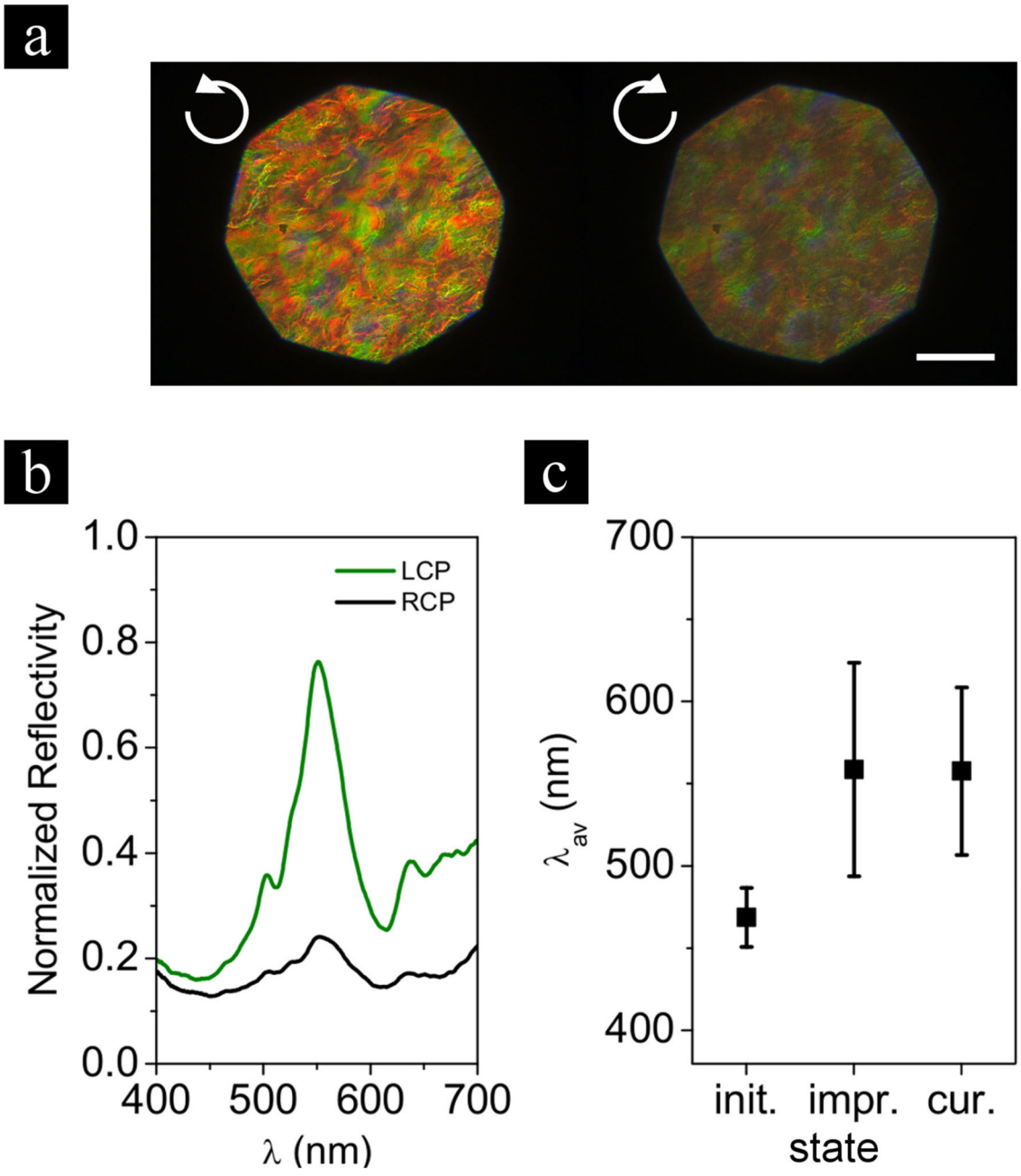

Figure 2.

a) Representative left (resp. right) circularly polarized (LCP, resp. RCP) optical micrographs of a hybrid CNC/PDDC-HD film obtained from a CNC film after impregnation with PDDC-HD prepolymer and curing treatment (obtained from initially blue CNC film). Scale bar corresponds to 100 μm. b) Reflectance spectra after curing. c) Evolution of the spectral position of λ_{av} throughout the different fabrication steps: initial, impregnation with PDDC-HD prepolymer and after PDDC-HD curing (error bars correspond to statistical standard deviation).

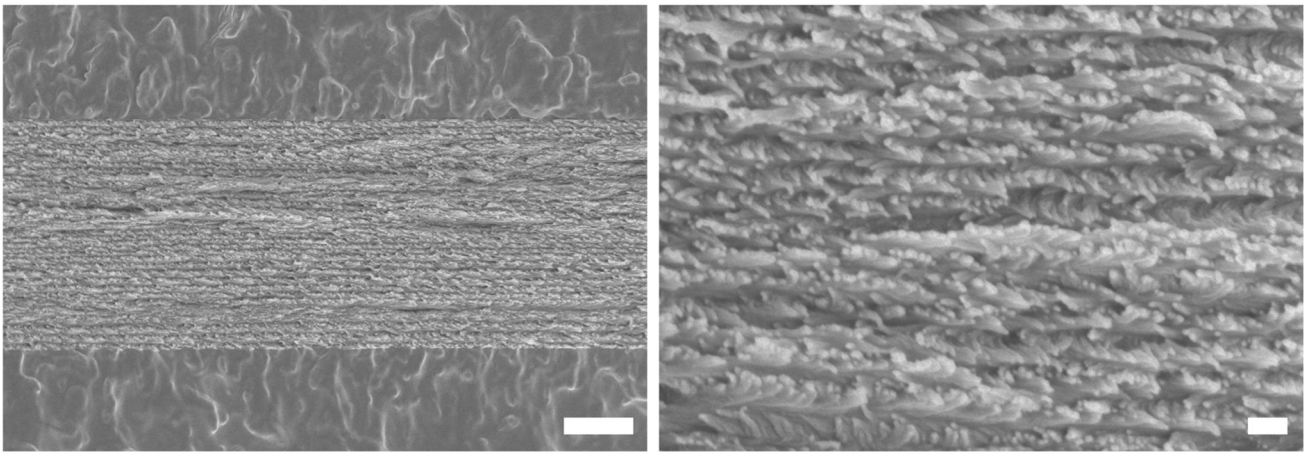

Figure 3.
Representative SEM cross-section images of a CNC/PDDC-HD hybrid material after impregnation of the prepolymer and curing. On the left, the elastomer layers surrounding both sides of the CNC film. On the right, the arrangement of the cellulose nanocrystals into a chiral nematic structure. Scale bars are 2 μm (left) and 200 nm (right).

Europe PMC Funders Author Manuscripts

Europe PMC Funders Author Manuscripts

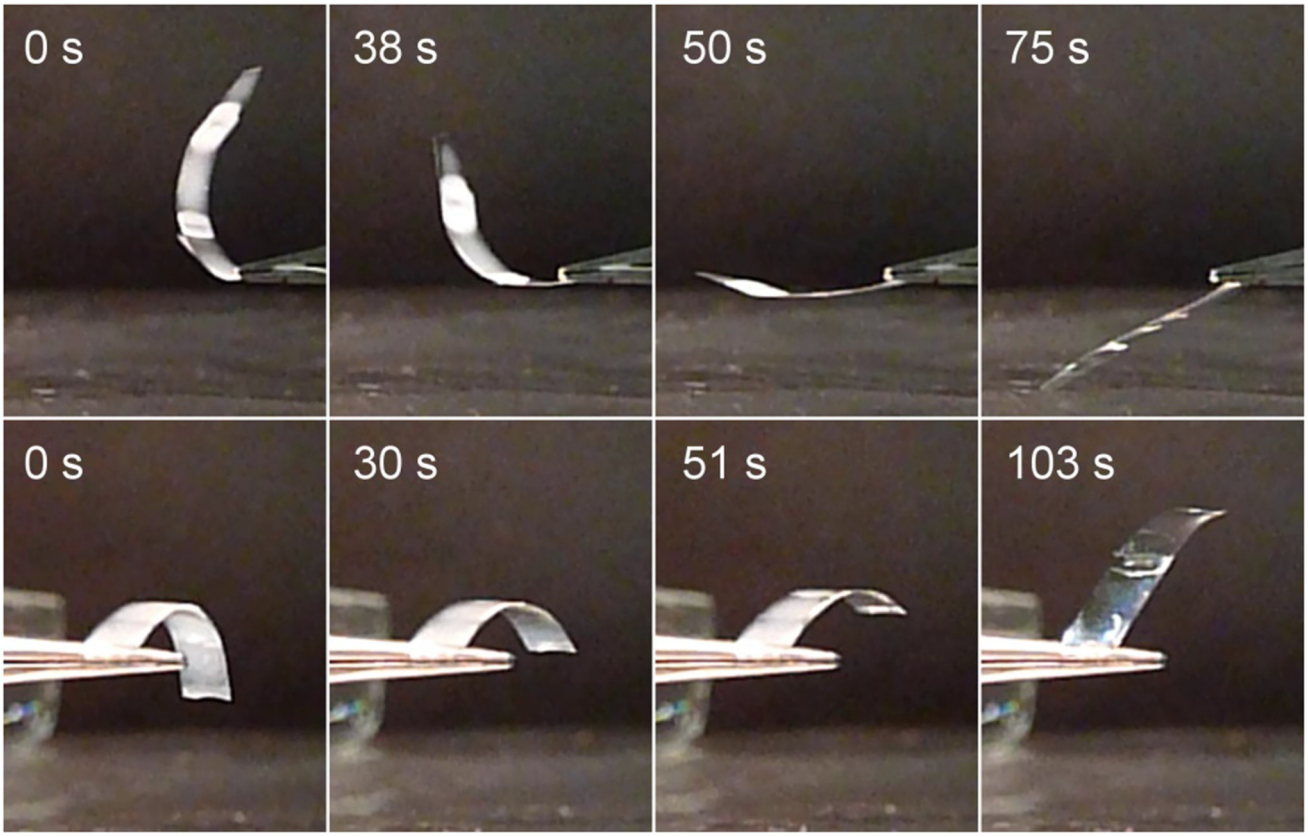

Figure 4.

Examples of thermomechanical cycles for the CNC/PDDC-HD composite, at four different times of the shape recovery process. The images at t = 0 s exhibits the temporary programmed shape. The top row corresponds to shape recovery in favor of gravity and the bottom one to a folding against it.

Europe PMC Funders Author Manuscripts

Table 1

Average spectral position of reflectance maxima (λ_{av}) along with average peak width (absolute FWHM - $\Delta\lambda_{av}$ and relative - $\Delta\lambda_{av}/\lambda_{av}$) of the left-circularly polarized Bragg peak, for the blue, green and red CNC films, before and after the prepolymer infiltration, prior to curing.

Initial film color	**Blue**			**Green**			**Red**		
	λ_{av} (nm)	$\Delta\lambda_{av}$ (nm)	$\Delta\lambda_{av}/\lambda_{av}$	λ_{av} (nm)	$\Delta\lambda_{av}$ (nm)	$\Delta\lambda_{av}/\lambda_{av}$	λ_{av} (nm)	$\Delta\lambda_{av}$ (nm)	$\Delta\lambda_{av}/\lambda_{av}$
initial	470 ± 20	61	13%	570 ± 20	39	7%	630 ± 70	80	13%
impregnated	560 ± 70	102	18%	660 ± 80	73	11%	700 ± 100	106	15%

Europe PMC Funders Author Manuscripts

Table 2

Detailed comparison of the physical properties of a sample before and after impregnation and curing, derived from SEM and optical analysis (case of an initially green sample).

		initial	cured	variation
Thickness t_{layer} by SEM (μm)	PDDC-HD top layer	--	21 ± 0.5	N.D.
	CNC middle layer	4.5 ± 0.3	6.5 ± 0.5	+45%
	PDDC-HD bottom layer	--	6 ± 0.3	N.D.
Pitch by SEM (nm)	Pitch average	355	412	+16%
	Pitch std dev	55	82	+50%
Spectral analysis	λ_{av} (nm)	570	660	+16%
Fabry-Perot oscillations	$n_{av} * t_{av}$ (nm)	5.27	5.73	+8.7%